# Distributed quantum sensing with optical lattices

Jose Carlos Pelayo,* Karol Gietka, and Thomas Busch
*Quantum Systems Unit, Okinawa Institute of Science and Technology Graduate University, Okinawa 904-0495, Japan*

(Received 2 September 2022; revised 23 January 2023; accepted 15 February 2023; published 17 March 2023)

In distributed quantum sensing the correlations between multiple modes, typically of a photonic system, are utilized to enhance the measurement precision of an unknown parameter. In this work, we investigate the metrological potential of a multimode, tilted Bose-Hubbard system and show that it can allow for parameter estimation at the Heisenberg limit of $[N(M-1)T]^2$, where $N$ is the number of particles, $M$ is the number of modes, and $T$ is the measurement time. The quadratic dependence on the number of modes can be used to increase the precision compared to typical metrological systems with only two atomic modes and does not require correlations between different modes. We show that the limit can be reached by using an optimized initial state given as the superposition of all the atoms occupying the first and last sites. Subsequently, we present strategies that would allow us to obtain quadratic dependence on $M$ of the Fisher information in a more realistic experimental setup.

DOI: 10.1103/PhysRevA.107.033318

## I. INTRODUCTION

The main aim of quantum metrology is to understand how utilizing quantum effects can enhance the estimation precision of a parameter beyond the classical limits [1–4]. The latter is given by the shot-noise limit (SNL), which restricts the estimation precision to scale as $\Delta\theta \sim (N\nu)^{-\frac{1}{2}}$, where $\theta$ is a parameter one wishes to measure precisely, $N$ is the number of particles being measured, and $\nu$ is the number of measurement repetitions. Making use of entangled states, one can enhance the precision by a factor of $k^{-\frac{1}{2}}$, where $k$ is the number of entangled particles [5], and in the limit of a maximally entangled many-body state, i.e., when $k = N$, one can achieve an estimation precision which scales as $N^{-1}\nu^{-\frac{1}{2}}$ for a decoherence-free system. This is the so-called *Heisenberg scaling*, which provides an improvement of $\sim N^{-\frac{1}{2}}$ over the SNL [6]. The metrological enhancement over the SNL has been demonstrated by utilizing entangled states such as squeezed states [7,8], NOON states [9], and others [6,10–12] and has been implemented using a variety of setups such as squeezed-state interferometers [13,14], cavity QED [15–17], ion traps [18–20], and distributed quantum networks [21–24]. In distributed quantum networks, a single-mode photonic input state is fed to a global beam-splitter network which consists of $M$ modes. The output state is then correlated between all of the modes before the parameter is imprinted and then measured at each mode. In this protocol, the parameter estimation has been shown to scale as $M^{-1}$, which corresponds to Heisenberg-like scaling for the system. This demonstrates that aside from scaling with the number of particles, one can also utilize scaling with the number of modes to further enhance the parameter estimation.

In standard setups for distributed quantum networks for photons, multimode correlations can be readily created through the use of beam splitters. However, in recent years precise control of atomic systems has become possible as well through the advent of atom-cooling, -trapping, and -engineering techniques [25–27]. Despite this, atomic systems have received relatively little attention in the context of distributed quantum networks [28], and in this work, we want to bridge that gap and explore the metrological applications of multimode cold atomic systems by investigating how one can enhance the estimation precision by manipulating the controllable parameters of atoms trapped in an optical lattice.

## II. HEISENBERG LIMIT IN MULTIMODE, MULTIPARTICLE ATOMIC SYSTEMS

The ultimate bound to the estimation precision for a parameter $\theta$ over all possible measurements is given by the quantum Cramér-Rao bound, $\Delta\theta \geqslant \Delta\theta_{\mathrm{QCR}} = 1/\sqrt{\nu F(\theta)}$, where $F(\theta)$ is the quantum Fisher information [29,30]. Given a Hamiltonian $H_\theta$ that depends on the parameter $\theta$ and evolves in time according to $U_\theta = \exp(-iH_\theta t)$, one can determine the quantum Fisher information by introducing a local generator $\hat{h}_\theta = i(\partial_\theta U_\theta)U_\theta^\dagger$, which characterizes the sensitivity of a state $\rho_\theta$ to an infinitesimal change in $\theta$, from $\rho_\theta \to \rho_{\theta+d\theta}$. For a system with an initial state that is a pure state $|\psi\rangle$, the quantum Fisher information can then be written as $F(\theta) = 4\langle\psi|\Delta^2\hat{h}_\theta|\psi\rangle$ [29,31], and it is maximized when the initial state is given by an optimal state of the form $|\psi_{\mathrm{opt}}\rangle = \frac{1}{\sqrt{2}}(|h_{\max}\rangle + |h_{\min}\rangle)$. In this case one gets

$$F_{\max}(\theta) = (h_{\max} - h_{\min})^2, \tag{1}$$

*jose-pelayo@oist.jp

where $h_{\max}$ and $h_{\min}$ are the maximal and minimal eigenvalues of $\hat{h}_\theta$ associated with states $|h_{\max}\rangle$ and $|h_{\min}\rangle$, respectively [4]. In the case where the Hamiltonian is composed of noncommuting terms, a compact expression for the local generator may not be available. An alternative expression to the local generator can be written in terms of the eigenvalues $E_k$ and eigenvectors $|\phi_k\rangle$ of the Hamiltonian [32], given as

$$\hat{h}_\theta = \hat{h}_\theta^{(L)} + \hat{h}_\theta^{(O)}, \tag{2}$$

$$\hat{h}_\theta^{(L)} = t \sum_{k=1}^{n_s} \frac{\partial E_k}{\partial \theta} |\phi_k\rangle\langle\phi_k|, \tag{3}$$

$$\hat{h}_\theta^{(O)} = 2 \sum_{l\neq k} e^{-\frac{itE_{kl}}{2}} \sin\left(\frac{tE_{kl}}{2}\right) \langle\phi_l|\partial_\theta\phi_k\rangle |\phi_k\rangle\langle\phi_l|, \tag{4}$$

where $E_{kl} = E_k - E_l$ and $n_s$ is the total number of states, while $\hat{h}_\theta^{(L)}$ and $\hat{h}_\theta^{(O)}$ are the linear and oscillating parts of the local generator, respectively. Note that we use the convention $\hbar = 1$ throughout the paper.

To describe a multiparticle, multimode atomic system let us first consider a general Hamiltonian of the form

$$H = \gamma \sum_m m \hat{a}_m^\dagger \hat{a}_m, \tag{5}$$

where $\gamma$ is the parameter we wish to measure precisely, $\hat{a}_m^\dagger$ and $\hat{a}_m$ are creation and annihilation operators, and the mode label $m$ runs from 1 to $M$. The quantum Fisher information for a system described by Hamiltonian (5) is maximized by a state

$$|\psi_{\text{opt}}\rangle = \frac{1}{\sqrt{2}}(|N0\cdots0\rangle + |0\cdots0N\rangle), \tag{6}$$

which is a superposition of all the atoms occupying the first and last sites (for the sake of brevity we will call this a generalized NOON state), and can be calculated to be

$$F_{\max}(\gamma) = T^2[N(M-1)]^2 = F_{\text{HL}}, \tag{7}$$

where $T$ is the length of the time interval during which the information about the unknown parameter was being imprinted. This will be our definition of the Heisenberg limit $F_{\text{HL}}$ throughout this work. In particular, we will consider a one-dimensional (1D) lattice system in a uniform linear potential, where $M$ is the total number of lattice sites, such that the enhancement proportional to $(M-1)$ is reminiscent of the scaling obtained from distributed photonic networks where $M$ refers to the number of modes. However, in the photonic systems, the maximum quantum Fisher information scales with $\sim\bar{n}M^2$, where $\bar{n} \equiv N/M$ is the average photon number per mode [21]. Thus, once the Fisher information is expressed in terms of the total number of photons $N$, the quadratic dependence on the number of modes disappears. In the following, we propose a possible realization of such a system using cold atoms and explore different strategies that can take advantage of the presence of multiple modes.

## III. TILTED BOSE-HUBBARD MODEL

A Hamiltonian with a term given in Eq. (5) can be realized in a one-dimensional lattice system that is exposed to a uniform linear potential. Such a system is also known as a tilted

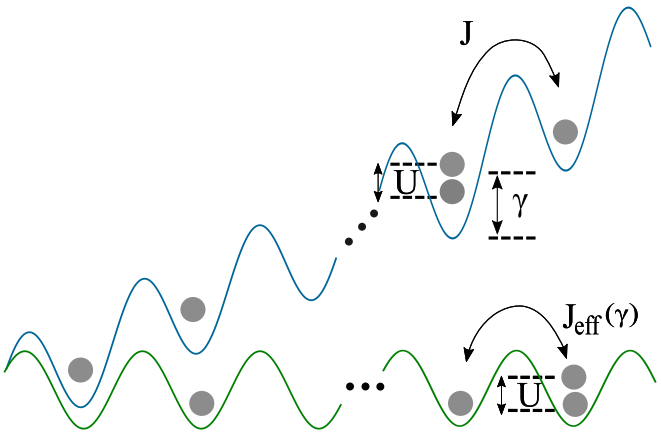


FIG. 1. Top: Schematic of the TBH model. Bottom: Schematic of the driven TBH model in the effective time-independent picture as given in Eq. (10). All parameters in Eq. (10) are scaled with respect to the tunneling coefficient $J$ and are fixed for all simulations (except for $U$) with the following values: $J = 1$, $\gamma = 33J$, $V_0 = 30.4J$, $\theta = \pi$, $\phi_{m+1} = \phi_m - \pi$, and $\phi_0 = -\pi/2$.

Bose-Hubbard (TBH) model and can be described by

$$H_{\text{TBH}} = -J \sum_{\langle i,j\rangle} \hat{a}_i^\dagger \hat{a}_j + \gamma \sum_j j\hat{n}_j + \frac{U}{2} \sum_j \hat{n}_j(\hat{n}_j - 1), \tag{8}$$

where $J$ is the tunneling coefficient, $\langle\cdot\rangle$ denotes nearest-neighbor sites, $U$ quantifies the on-site interaction strength between the particles, $\gamma$ is the strength of the tilt, and $\hat{n}_m = \hat{a}_m^\dagger \hat{a}_m$ is the number operator. A schematic of the system is shown in Fig. 1 (top), and we assume that we have only a finite number of sites, $j = 1, \ldots, M$. Although the TBH Hamiltonian contains additional terms when compared to Eq. (5), it is known that terms that are not dependent on the unknown parameter cannot alter the maximum attainable precision [33]. Thus, the Bose-Hubbard system in Eq. (8) will have a maximum quantum Fisher information that is still bounded by Eq. (7).

The Hamiltonian in Eq. (8) can be realized using ultracold atoms trapped in a 1D optical lattice under the influence of a linear potential of strength $\gamma$, which, for example, can be gravitational or magnetic in nature [34–36]. Therefore, a precise measurement of the parameter $\gamma$ would correspond to making a precise measurement of the gravitational acceleration or magnetic field gradient. The interaction strength $U$ can be tuned by employing Feshbach resonances [37,38] and is designed to be small relative to $\gamma$ such that excitations to higher bands are suppressed.

Assuming one can prepare the generalized NOON state in Eq. (6) at $t = 0$, the interaction can then be set to $U = 0$, and the lattice depth can be set to a value such that $J \ll \gamma$, which freezes the spatial dynamics. The remaining dynamics is therefore purely in the phase difference between the two states in the superposition and is of the form $|\psi_{\text{opt}}(t)\rangle \sim \frac{1}{\sqrt{2}}(|N0\cdots0\rangle + e^{-it\gamma N(M-1)}|0\cdots0N\rangle)$, which is a state that yields $F_{\text{HL}}$ at all times. In this case, all the information about the unknown parameter is stored in the relative phase between the two components of the wave function. It could be retrieved, for example, by performing an interference

measurement, i.e., transferring the information stored in the relative phase to the occupation of each site, which might be experimentally challenging. Furthermore, NOON states are known to be very fragile against losses and thus difficult to prepare. Although several approaches have been suggested in the literature, especially for two-site systems, they usually suffer from having low fidelity as the number of particles is increased [39–43]. We therefore explore in the following the prospects for metrology with a TBH model using a more realistic initial state.

## IV. FISHER INFORMATION WITH AN INITIAL FOCK STATE

Let us start by considering an initial state where the particles are all placed in the lowest-energy site of the lattice

$$|\psi_{\text{Fock}}\rangle = |N0\cdots0\rangle. \tag{9}$$

We first investigate the case where interactions are switched off and show later that, when $U > 0$, additional improvement to the quantum Fisher information can be observed due to the correlations introduced by the interactions.

Given that $\gamma \gg J$, the spatial dynamics is frozen as before, and since $4\langle\psi_{\text{Fock}}|\Delta^2\hat{h}_\theta|\psi_{\text{Fock}}\rangle = 0$, the Fisher information will be fixed to this value unless one restores the spatial dynamics. To introduce atomic dynamics to the system that depends on $\gamma$, we therefore consider a periodic drive with frequency $\omega = \gamma$, which involves knowledge about the unknown parameter. Such an approach would require, for example, an adaptive protocol where the knowledge about $\omega$ would be updated with every round of the protocol [44–47]. The driven Hamiltonian can then be written as

$$H_{\text{DBH}} = H_{\text{TBH}} + V_0 \sum_m \hat{n}_m \sin\left(\omega t + \phi_m + \frac{\theta}{2}\right), \tag{10}$$

where $V_0$ is the driving amplitude, $\phi$ is a site-dependent phase, and $\theta$ is a constant phase. A schematic of the driven system in the effective time-independent picture is shown in Fig. 1 (bottom). These kinds of driving terms can be experimentally realized by an off-resonant laser-assisted tunneling scheme [35,48]. In order to suppress decoherence due to particle loss into the higher bands we choose our driving parameters based on a stability diagram shown in Appendix A and focus on the limit $\gamma \gg U$ [49,50]. The resulting quantum Fisher information [51] of the system in Eq. (10) is computed using

$$F(\gamma) = 4(\langle\partial_\gamma\psi_\gamma|\partial_\gamma\psi_\gamma\rangle - |\langle\psi_\gamma|\partial_\gamma\psi_\gamma\rangle|^2). \tag{11}$$

Figure 2(a) shows the evolution of the quantum Fisher information $F^{(M)}$ using the initial state $|\psi_{\text{Fock}}\rangle$ in the noninteracting driven TBH model, where $M$ denotes the total number of lattice sites. Here, $F^{(M)}$ is scaled by $T^2$, and the number of particles is set to $N = 1$ as it makes only a linear contribution to the quantum Fisher information in the case of $U = 0$, that is, $F^{(M,N)} = NF^{(M)}$. The inset in Fig. 2(a) shows the oscillating behavior of the unscaled $F^{(M)}$ with $T$, and thus, in the vicinity of the first peak, $F^{(M)}$ starts to scale poorly compared to $T^2$. This means that we need to consider the dynamics only up until the first peak of $F^{(M)}/T^2$, and we denote this peak as $F^{(M)}_{\text{max}} = \max(F^{(M)}/T^2)$. Defining the time at which

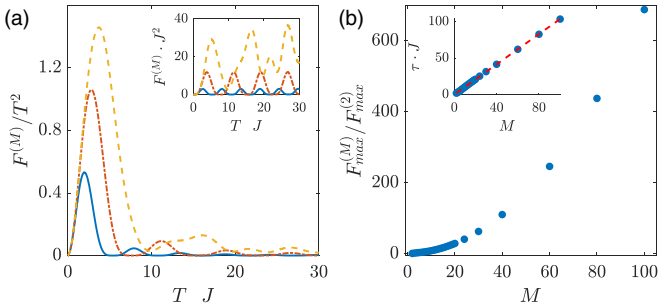


FIG. 2. (a) Time dependence of the scaled $F^{(M)}$ for $M = 2, 3, 4$, corresponding to the blue solid line, red dashed-dotted line, and orange dashed line, respectively (the unscaled $F^{(M)}$ is shown in the inset). (b) Growth of $F^{(M)}_{\text{max}}$ scaled by $F^{(M=2)}_{\text{max}}$ with $M$. The inset shows the linear scaling of $\tau$ with respect to $M$. (See text for details.)

$F^{(M)}_{\text{max}}$ is attained as $\tau$, one can see in the inset in Fig. 2(b) that it has a linear dependence on $M$ since more modes increase the time after which the state is transferred to the other end of the lattice. The quantum Fisher information enhancement relative to a two-level system $F^{(M)}_{\text{max}}/F^{(M=2)}_{\text{max}}$ is shown in Fig. 2(b) and clearly shows a quadratic dependence on $M$ for $M \gg 1$.

## V. EFFECT OF INTERACTIONS

Next, we will consider an interacting system in which nonclassical correlations can be created that should improve the quantum Fisher information. The initial state is the same as in the previous section, and we imprint the information about the unknown parameter and create the correlations at the same time [52,53]. A representative surface plot of the evolution of $F^{(M,N)}/T^2$ with varying interaction strength $U$ for $N = M = 3$ is shown in Fig. 3(a). Like in the noninteracting case, we also observe a sinusoidal-like evolution of $F^{(M,N)}$; therefore, we limit our interest up to the time $\tau$ when the first peak of $F^{(M,N)}/T^2$ appears. What is notable, however, is that a certain value of the interaction strength exists, which we will call $\bar{U}$, where the increase in $F^{(M,N)}$ over the noninteracting case is maximal. For the parameters used in Fig. 3(a) this corresponds to $\bar{U} \approx 1.92J$, and in general, we observe an increase of $F^{(M,N)}_{\text{max}}$ as $N$ and $M$ increase [see Fig. 3(b)]. When $F^{(M,N)}_{\text{max}}$ is compared to a two-level system $F^{(M=2,N)}_{\text{max}}$, we still observe an enhancement as $M$ increases; however, increasing the number of particles may not always yield a larger enhancement, as shown in Fig. 3(c). Finally, when $F^{(M,N)}_{\text{max}}$ is compared to the Heisenberg limit, the two-level system yields a stronger enhancement over any $M > 2$ (for small $M$), and we again observe that the increase in $N$ does not always provide a larger enhancement, as can be seen in Fig. 3(d). While it might look like that for an increasing number of modes $F^{(M,N)}_{\text{max}}/F_{HL} \to\sim 0.2$, our limited computational resources currently do not allow us to explore this.

To better understand the behavior of the quantum Fisher information $F^{(M,N)}$, we take the high-frequency approximation [49,50,54,55] of the driven, tilted Bose-Hubbard model up to first order in $1/\omega$, which leads to an effective,

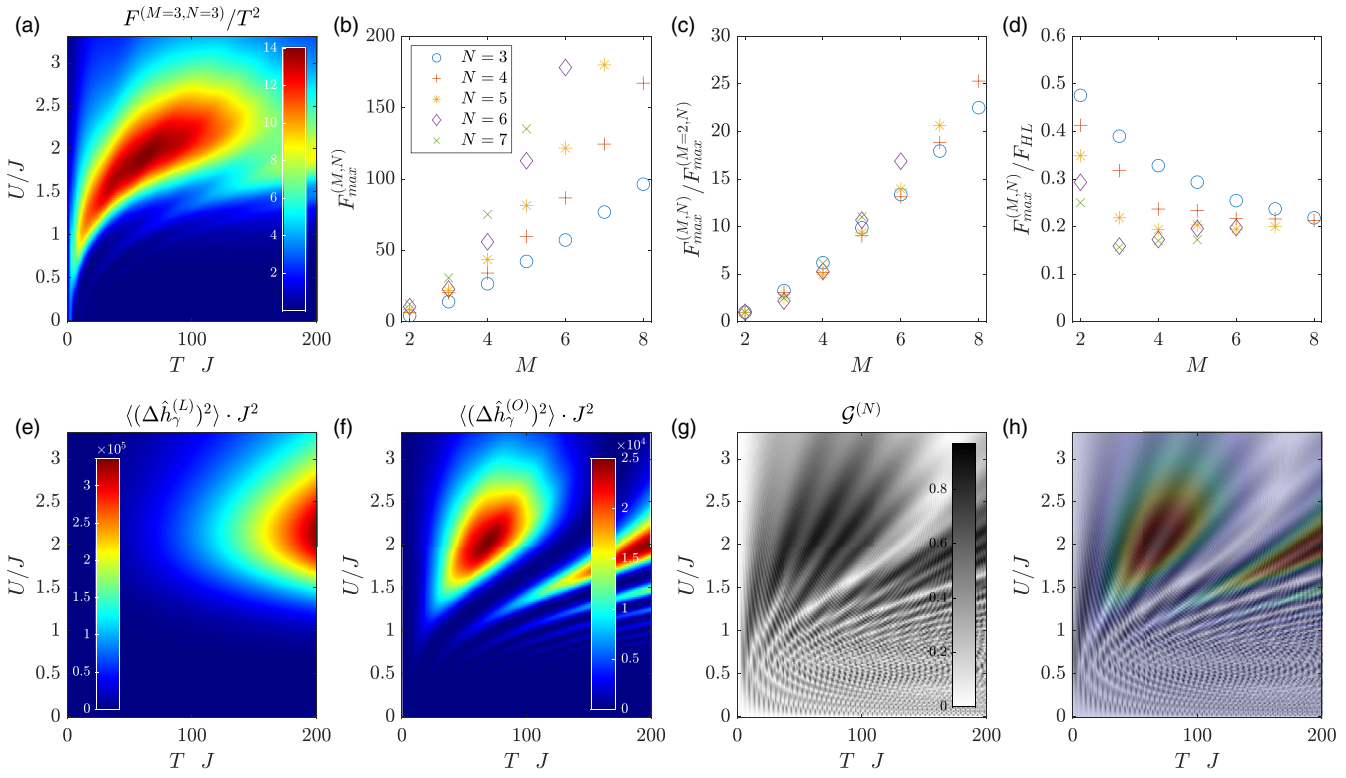


FIG. 3. (a) Density plot of the scaled $F^{(M,N)}$ as a function of $T$ and $U$ for $N = M = 3$. (b) Growth of $F_{\max}^{(M,N)}$ with $M$ for $N = 3, 4, 5, 6, 7$. The legend applies for (b)–(d). $F_{\max}^{(M,N)}$ (c) scaled by $F_{\max}^{(M=2,N)}$ and (d) scaled by the Heisenberg limit. Shown in (c) and (d) are all the data points that we were able to numerically obtain. (e) and (f) The variance of $\hat{h}_\gamma^{(L)}$ and $\hat{h}_\gamma^{(O)}$, respectively. In (g) the correlation function $\mathcal{G}^{(N)}$ is calculated for varying $U$ and $T$, and (h) shows the variance of $\hat{h}_\gamma^{(O)}$ overlaid by the correlation function. (See text for details.)

time-independent description of the system, given as

$$H_{\text{eff}} = -J_F \sum_j (\hat{a}_{j+1}^\dagger \hat{a}_j e^{-i\phi_j} + \text{H.c.}) + \frac{U}{2}\sum_j \hat{n}_j(\hat{n}_j - 1) + K\left(\frac{1}{\omega}\right)\sum_j (\hat{n}_{j+1} - \hat{n}_j) + O\left(\frac{1}{\omega^2}\right), \tag{12}$$

where $J_F = J\mathcal{J}_1(2V/\omega)$ is the renormalized tunneling coefficient and $\mathcal{J}_1(x)$ is a Bessel function of the first kind. Since the effective Hamiltonian in Eq. (12) is time independent, the Fisher information can now be calculated from the local generator $\hat{h}_\gamma$ using Eq. (2), and we look at the contributions from the linear part $\hat{h}_\gamma^{(L)}$ and the oscillating part $\hat{h}_\gamma^{(O)}$ separately. The respective variances are plotted in Figs. 3(e) and 3(f), and one can see that $\langle(\Delta\hat{h}_\gamma^{(L)})^2\rangle$ dominates over $\langle(\Delta\hat{h}_\gamma^{(O)})^2\rangle$ at long times due to its quadratic dependence on time. The sinusoidal-like behavior that is seen in the inset in Fig. 2(a) originates from $\langle(\Delta\hat{h}_\gamma^{(O)})^2\rangle$, and $\tau$ sets the timescale for the appearance of the first maximum of this term. The dependence of these generators on the eigenstates of $H_{\text{eff}}$ is discussed in Appendix B.

Finally, to illustrate that this enhancement of the quantum Fisher information is related to an increase in nonclassical correlations, we make use of the $N$th-order correlation function, given as [56]

$$\mathcal{G}^{(N)} = \left|\frac{1}{C}\langle\psi(t)|(\hat{a}_M^\dagger \hat{a}_1)^N|\psi(t)\rangle\right|, \tag{13}$$

where $C = N!/2$ is a normalization constant. $\mathcal{G}^{(N)}$ quantifies the $N$-particle correlation between the two outermost sites, $j = 1, M$. One can show that for a generalized NOON state $|\psi_{\text{opt}}(t)\rangle$, the correlation function is $\mathcal{G}^{(N)} = 1$ at all times. On the other hand, for an initial Fock state $|\psi_{\text{Fock}}\rangle$, that is not the case. A surface plot of $\mathcal{G}^{(N)}$ as a function of $(T, U)$ is shown in Fig. 3(g) for $|\psi_{\text{Fock}}\rangle$ and $M = N = 3$. One can see that $\mathcal{G}^{(N)}$ has the same qualitative features as $\langle(\Delta\hat{h}_\gamma^{(O)})^2\rangle$, and by superimposing $\langle(\Delta\hat{h}_\gamma^{(O)})^2\rangle$ on $\mathcal{G}^{(N)}$ [see Fig. 3(h)] one can see that the maxima of $\langle(\Delta\hat{h}_\gamma^{(O)})^2\rangle$ lie in the region of large $\mathcal{G}^{(N)}$. This comparison, however, does not always hold true, as can be seen for small $U$ when the correlator $\mathcal{G}^{(N)}$ suggests that there can be a large correlation but the quantum Fisher information is relatively small. However, we have confirmed that for all combinations of $N = 3, 4, 5$ and $M = 3, 4$ the regions of large $\langle(\Delta\hat{h}_\gamma^{(O)})^2\rangle$ also correspond to large correlations (not shown). As one goes to larger $N$ for a fixed $M$, the maximum correlation no longer approaches unity, which could explain why the scaled $F_{\max}^{(M,N)}$ in Figs. 3(c) and 3(d) does not always increase even if $N$ is increased for a fixed $M$.

## VI. CONCLUSIONS

In this work, we have investigated the use of a multimode atomic system in the context of distributed quantum sensing. We have shown that the driven, tilted Bose-Hubbard model can make use of the additional degree of freedom of the number of lattice sites or number of modes $M$ in order to

increase the quantum Fisher information of the system with respect to some unknown parameter responsible for the tilt (for example, gravitational acceleration could be a natural candidate). A generalized NOON state maximizes the quantum Fisher information at all times when the spatial dynamics is frozen; however, extracting information from such a state might require a complicated measurement procedure. An initial Fock state cannot saturate the Heisenberg limit but can still benefit from the quadratic scaling in $M$. In this case, the occupation of each site can be used as an optimal estimator since no information about the unknown parameter is being stored in the phase [57]. This quadratic scaling was made possible through the introduction of the periodic drive, with a period related to the unknown parameter, which translates the information about the parameter into the tunneling dynamics of the particles. On the other hand, for a distributed photonic network, its quadratic scaling in $M$ becomes linear once the quantum Fisher information is expressed in terms of the total number of particles. Additionally, by introducing interactions to the system we have shown that parameter imprinting and the creation of correlations can be achieved simultaneously, in contrast to distributed photonic networks, where the creation of the correlated state is performed before parameter imprinting.

We emphasize that the enhancement with respect to the number of modes is not an unexpected result. Suppose we have a harmonic oscillator where the energy spacing is $\omega_0$, and suppose further that there is a nonlinear process that can drive the system from the ground state to the $M$th level with energy $\omega_M = M\omega_0$; then using the error propagation formula, we find that the uncertainty in $\omega_0$ is given by $\Delta\omega_0 = \Delta\omega_M/M$. This is the same enhancement we observe for the tilted, Bose-Hubbard model using the generalized NOON state. The only difference here is that no nonlinear process is used to couple neighboring modes, which thus demonstrates the advantage of utilizing a ladderlike system with multiple modes in metrology. It is clear that the existence of the tilt (or any dispersion which is of the form $m^\alpha$, where $\alpha \geqslant 1$ and $m$ is the mode index) is what allows the enhancement with the number of modes; therefore, other ladderlike systems can also exploit this enhancement. That said, we would like to stress that the enhancement with $M$ is rather classical as it can be simply related to the increased size of the lattice. An example of such a system is the periodically forced Bose-Hubbard model [58], given as $H_{\mathrm{PF}} = H_0 + \Gamma\cos(\omega t)\sum_j j\hat{n}_j$, where the difference between this and the tilted Bose-Hubbard model is that the tilt is no longer linear but instead is periodic in time. What is interesting here is that if we precisely measure $\omega$ instead of $\Gamma$, we find that the Heisenberg limit is $(\Gamma NM)^2T^4$, where we still have the enhancement in $N$ and $M$ but now the scaling with time is superquadratic and can be achieved only if one incorporates an additional optimal control Hamiltonian [51]. These ladderlike systems provide an avenue to study quantum metrological setups which have the potential to further increase precision measurements.

## ACKNOWLEDGMENTS

The authors would like to acknowledge L. Ruks for fruitful discussions. Simulations were performed using the open-source QUANTUMOPTICS.JL framework in Julia [59]. The authors acknowledge support from the Okinawa Institute of Science and Technology (OIST) Graduate University and from Japan Society for the Promotion of Science (JSPS) Grant-in-Aid for Scientific Research (C) No. 20K03795. The authors are also grateful for the Scientific Computing and Data Analysis (SCDA) section of the Research Support Division at OIST.

## APPENDIX A: FLOQUET FERMI'S GOLDEN RULE

The discussion below of the Floquet Fermi's golden rule for the driven, tilted Bose-Hubbard model closely follows Ref. [60]. The key assumption here is that the interaction strength $U$ must satisfy $U \ll V_0, \omega$ such that the interaction term can be treated using a perturbative scattering theory. We consider a two-band, tilted, driven Bose-Hubbard model without interaction,

$$\begin{aligned} H = &-\sum_{<i,j>}\left(J^{(a)}\hat{a}_i^\dagger\hat{a}_j + J^{(b)}\hat{b}_i^\dagger\hat{b}_j\right) + \gamma\sum_j j\left(\hat{a}_j^\dagger\hat{a}_j + \hat{b}_j^\dagger\hat{b}_j\right) \\ &+ V_0\sum_j \sin\left(\omega t + \phi_j + \frac{\theta}{2}\right)\left(\hat{a}_j^\dagger\hat{a}_j\right. \\ &\left.+ \hat{b}_j^\dagger\hat{b}_j\right) + \Delta_g\sum_j \hat{b}_j^\dagger\hat{b}_j. \end{aligned} \tag{A1}$$

Here, $\hat{b}^\dagger$ ($\hat{b}$) corresponds to the creation (annihilation) operator of the second band, and $J^{(a)}$ and $J^{(b)}$ are the tunneling coefficients in the first and second bands, respectively. The energy gap between the two bands is $\Delta_g$ and is the largest energy scale in the system, $\Delta_g > V_0, \gamma \approx \omega \gg J^{(a)}, J^{(b)}$. The system is diagonalized in momentum space by introducing $\hat{a}_k = (1/\sqrt{M})\sum_m e^{(-ikx_m)}\hat{a}_m$ and $\hat{a}_k^\dagger = (1/\sqrt{M})\sum_m e^{(ikx_m)}\hat{a}_m^\dagger$, where $k$ is the quasimomentum and $x_m = md$, with $d$ being the lattice spacing. This gives the quasienergies

$$\begin{aligned} E^{(a)}(\kappa) &= \pm 2J_F^{(a)}\cos(\kappa), \\ E^{(b)}(\kappa) &= \pm 2J_F^{(b)}\cos(\kappa) + \Delta_g, \end{aligned} \tag{A2}$$

where $J_F^{(\beta)} = J^{(\beta)}\mathcal{J}_1(2V/\omega)$ is the renormalized tunneling coefficient with $\beta = \{a, b\}$ and $\kappa = kd$ is a dimensionless quasimomentum. Following Ref. [60], one can define a transition rate from an initial state to a final state $\gamma_{i\to f}$. If the initial state is in the first band and the final state is in the second band, this corresponds to the scattering of particles to a higher band mediated by the absorption of energy $m\omega$ coming from the periodic drive, where $m$ is an integer. In the context of Floquet-engineered systems, this is considered a heating process that we try to suppress using suitable driving parameters $\{V_0, \omega\}$. The expression for the Floquet Fermi's golden rule can be written as

$$\begin{aligned} \gamma_{i\to f} = &\sum_{m,\alpha,\beta} |c_\beta c_\alpha|^2 \frac{2\pi}{\hbar}\delta(E^{(\alpha)} - E^{(\beta)} - m\omega) \\ &\times \left|\left\langle\!\left\langle \Phi_\beta^m \middle| \hat{V} \middle| \Phi_\alpha \right\rangle\!\right\rangle\right|^2, \end{aligned} \tag{A3}$$

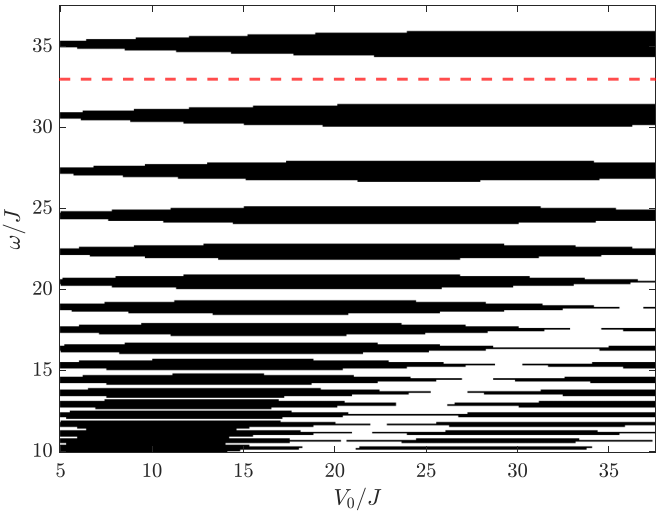


FIG. 4. Stability diagram depicting the resonance condition for a given $\{\omega, V_0\}$ shown with the black shading. The orange dashed line indicates the drive frequency $\omega$ we used in the simulations. The parameters are $J^{(a)} = 1$, $J^{(b)} = 1.5J$, and $\Delta g = 123J$.

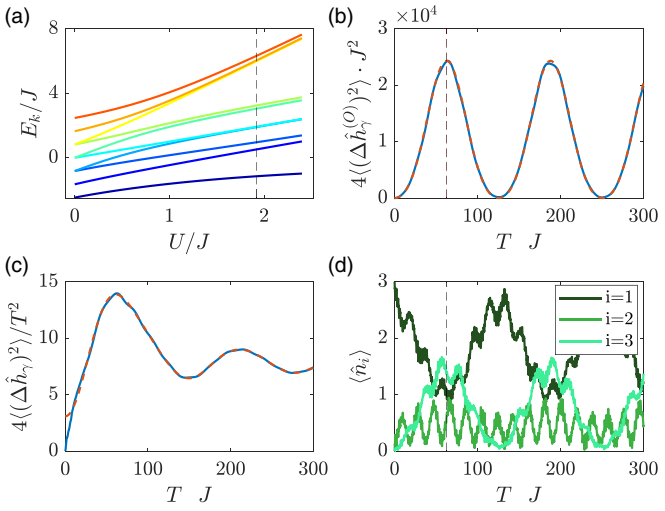


FIG. 5. The plots are determined for the case $M = N = 3$. In (a) the eigenvalues $E_k$ are shown as a function of increasing interaction strength $U$. The lowest line corresponds to the ground-state energy. In (a) the vertical dashed line corresponds to $U = \bar{U}$, while in (b) and (d) the vertical dashed line corresponds to $T = \tau$. In (b) and (c) the variances $\langle(\Delta\hat{h}_\gamma^{(O)})^2\rangle$ and $\langle(\Delta\hat{h}_\gamma)^2\rangle/T^2$ as a function of $T$ are calculated using the full oscillating generator $\hat{h}_\gamma^{(O)}$ (blue solid line) and the approximate generator $\tilde{\hat{h}}_\gamma^{(O)}$ (orange dashed line). (d) The site occupation number $\langle\hat{n}_j\rangle$ is plotted as a function of $T$. (b)–(d) are calculated at fixed $U = \bar{U}$. (See text for details.)

where $|\Phi_\beta^m(t)\rangle = e^{im\omega t}|\Phi_\beta(t)\rangle$ and the extended scalar product is defined as $\langle\langle u|v\rangle\rangle = (1/T)\int_0^T dt\langle u(t)|v(t)\rangle$. Setting $\alpha = a$ and $\beta = b$ corresponding to energies $E^{(a)}$ and $E^{(b)}$ in Eq. (A2), the Floquet Fermi's golden rule in Eq. (A3) then indicates a transition from the lowest band to the next-lowest band is allowed through the absorption of $m$ photons given that an appropriate interaction term couples the two bands, $\langle\langle\Phi_b^m|\hat{V}|\Phi_a\rangle\rangle \neq 0$. We focus on the energy requirement in Eq. (A3) and assume that a scattering process can couple the two lowest bands and that an arbitrary number of photons can be absorbed. This leads us to the stability diagram shown in Fig. 4. The shaded regions correspond to $\{V_0, \omega\}$ for which the energy requirement above is satisfied and thus scattering of particles to higher bands is possible. The topmost region corresponds to an absorption of energy $m\omega = 7\omega$, and each succeeding region corresponds to an increase in absorbed energy by $+\omega$. Notice that as we decrease the drive frequency $\omega$, the gap between neighboring regions becomes smaller, and they can even overlap for specific values of the drive strength $V_0$. This illustrates that for our system, heating becomes prominent as we move away from the high-frequency limit. Although our initial state, $|\Psi_i(t_0)\rangle = \sum_\alpha c_\alpha e^{-iE_\alpha t_0}|\Phi_\alpha(t_0)\rangle$, and final state, $|\Psi_f(t)\rangle = \sum_\beta c_\beta e^{-iE_\beta t}|\Phi_\beta(t)\rangle$, are not eigenstates of the system, we argue that the relevant states here are found in the first and second bands and thus the stability diagram is still valid.

## APPENDIX B: EIGENDECOMPOSITION OF $H_{\text{eff}}$

Another perspective on the local generator and quantum Fisher information is to look at the eigenvalues $E_k$ and eigenfunctions $|\phi_k\rangle$ of the effective Hamiltonian in Eq. (12). In Fig. 5(a) we plot the energy of each of the eigenfunctions as a function of increasing interactions $U$, where the vertical dashed line corresponds to $U = \bar{U}$, at which we observe $F_{\max}^{(M,N)}$. One can see immediately that at this critical value, some of the eigenfunctions are close to degeneracy. This determines which terms in the sum in Eq. (4) are dominant when calculating $\langle(\Delta\hat{h}_\gamma^{(O)})^2\rangle$ since it contains $\langle\phi_l|\partial_\gamma\phi_k\rangle = \frac{\langle\phi_l|\frac{\partial H_{\text{eff}}}{\partial\gamma}|\phi_k\rangle}{E_k - E_l}$. While in Fig. 5(a) we see that there are two pairs of eigenfunctions that are close to being degenerate, only one of these pairs gives a large contribution and corresponds to the second- and third-largest eigenstates. The reason for this is that these two states, $|\phi_{n_s-1}\rangle$ and $|\phi_{n_s-2}\rangle$, correspond to the ones with the largest overlap with the initial Fock state, $|\langle\phi_{n_s-1}|\psi_{\text{Fock}}\rangle|^2 \approx 0.17$ and $|\langle\phi_{n_s-2}|\psi_{\text{Fock}}\rangle|^2 \approx 0.72$, respectively. The energy difference between this pair, $\Omega = E_{n_s-1} - E_{n_s-2}$, is then related to the oscillation frequency of $\langle(\Delta\hat{h}_\gamma^{(O)})^2\rangle$, and thus, one can approximate $\tau$ as $\tau \sim \frac{\pi}{\Omega}$ [see Fig. 5(b)]. The oscillating part of the local generator $\hat{h}_\gamma^{(O)}$ can then be approximated by just considering the states $|\phi_{n_s-1}\rangle$ and $|\phi_{n_s-2}\rangle$. We define this approximate generator as $\tilde{\hat{h}}_\gamma^{(O)}$, and its variance is also shown in Fig. 5(b). At long times this becomes a good approximation even when calculating the quantum Fisher information, as shown in Fig. 5(c). Finally, we determine the average occupation at each site $\langle\hat{n}_j\rangle$ as a function of $T$ for $U = \bar{U}$ [see Fig. 5(d)]. Here, we observe that at $T \sim \tau$ the average occupations between the first and last sites get close, which suggests that an observable such as $\sim\langle\hat{n}_1\rangle\langle\hat{n}_M\rangle$ can be a good estimator.

[1] V. Giovannetti, S. Lloyd, and L. Maccone, Advances in quantum metrology, Nat. Photon. **5**, 222 (2011).

[2] V. Giovannetti, S. Lloyd, and L. Maccone, Quantum-enhanced measurements: Beating the standard quantum limit, Science **306**, 1330 (2004).

[3] L. Pezze, A. Smerzi, M. K. Oberthaler, R. Schmied, and P. Treutlein, Quantum metrology with nonclassical states of atomic ensembles, Rev. Mod. Phys. **90**, 035005 (2018).

[4] V. Giovannetti, S. Lloyd, and L. Maccone, Quantum Metrology, Phys. Rev. Lett. **96**, 010401 (2006).

[5] L. Pezzé and A. Smerzi, Entanglement, Nonlinear Dynamics, and the Heisenberg Limit, Phys. Rev. Lett. **102**, 100401 (2009).

[6] J. J. Bollinger, W. M. Itano, D. J. Wineland, and D. J. Heinzen, Optimal frequency measurements with maximally correlated states, Phys. Rev. A **54**, R4649 (1996).

[7] D. J. Wineland, J. J. Bollinger, W. M. Itano, F. L. Moore, and D. J. Heinzen, Spin squeezing and reduced quantum noise in spectroscopy, Phys. Rev. A **46**, R6797 (1992).

[8] M. Kitagawa and M. Ueda, Squeezed spin states, Phys. Rev. A **47**, 5138 (1993).

[9] M. W. Mitchell, J. S. Lundeen, and A. M. Steinberg, Super-resolving phase measurements with a multiphoton entangled state, Nature (London) **429**, 161 (2004).

[10] P. Hyllus, W. Laskowski, R. Krischek, C. Schwemmer, W. Wieczorek, H. Weinfurter, L. Pezzé, and A. Smerzi, Fisher information and multiparticle entanglement, Phys. Rev. A **85**, 022321 (2012).

[11] R. Chaves, J. B. Brask, M. Markiewicz, J. Kołodyński, and A. Acín, Noisy Metrology Beyond the Standard Quantum Limit, Phys. Rev. Lett. **111**, 120401 (2013).

[12] G. Tóth, Multipartite entanglement and high-precision metrology, Phys. Rev. A **85**, 022322 (2012).

[13] R. S. Bondurant and J. H. Shapiro, Squeezed states in phase-sensing interferometers, Phys. Rev. D **30**, 2548 (1984).

[14] R. Schnabel, Squeezed states of light and their applications in laser interferometers, Phys. Rep. **684**, 1 (2017).

[15] K. Gietka, F. Mivehvar, and H. Ritsch, Supersolid-Based Gravimeter in a Ring Cavity, Phys. Rev. Lett. **122**, 190801 (2019).

[16] W. Cheng, S. C. Hou, Z. Wang, and X. X. Yi, Quantum metrology enhanced by coherence-induced driving in a cavity-QED setup, Phys. Rev. A **100**, 053825 (2019).

[17] R. J. Lewis-Swan, D. Barberena, J. A. Muniz, J. R. K. Cline, D. Young, J. K. Thompson, and A. M. Rey, Protocol for Precise Field Sensing in the Optical Domain with Cold Atoms in a Cavity, Phys. Rev. Lett. **124**, 193602 (2020).

[18] D. A. R. Dalvit, R. L. de Matos Filho, and F. Toscano, Quantum metrology at the Heisenberg limit with ion trap motional compass states, New J. Phys. **8**, 276 (2006).

[19] H. C. J. Gan, G. Maslennikov, K.-W. Tseng, T. R. Tan, R. Kaewuam, K. J. Arnold, D. Matsukevich, and M. D. Barrett, Oscillating-magnetic-field effects in high-precision metrology, Phys. Rev. A **98**, 032514 (2018).

[20] K. A. Gilmore, M. Affolter, R. J. Lewis-Swan, D. Barberena, E. Jordan, A. M. Rey, and J. J. Bollinger, Quantum-enhanced sensing of displacements and electric fields with two-dimensional trapped-ion crystals, Science **373**, 673 (2021).

[21] Q. Zhuang, Z. Zhang, and J. H. Shapiro, Distributed quantum sensing using continuous-variable multipartite entanglement, Phys. Rev. A **97**, 032329 (2018).

[22] W. Ge, K. Jacobs, Z. Eldredge, A. V. Gorshkov, and M. Foss-Feig, Distributed Quantum Metrology with Linear Networks and Separable Inputs, Phys. Rev. Lett. **121**, 043604 (2018).

[23] H. Kwon, Y. Lim, L. Jiang, H. Jeong, and C. Oh, Quantum Metrological Power of Continuous-Variable Quantum Networks, Phys. Rev. Lett. **128**, 180503 (2022).

[24] B. Zhou, A. J. Brady, and Q. Zhuang, Enhancing distributed sensing with imperfect error correction, Phys. Rev. A **106**, 012404 (2022).

[25] W. D. Phillips, Nobel lecture: Laser cooling and trapping of neutral atoms, Rev. Mod. Phys. **70**, 721 (1998).

[26] W. Ketterle and N. Van Druten, Evaporative cooling of trapped atoms, Adv. At., Mol., Opt. Phys. **37**, 181 (1996).

[27] H. J. Metcalf and P. van der Straten, Laser cooling and trapping of atoms, J. Opt. Soc. Am. B **20**, 887 (2003).

[28] B. K. Malia, Y. Wu, J. Martínez-Rincón, and M. A. Kasevich, Distributed quantum sensing with mode-entangled spin-squeezed atomic states, Nature **612**, 661 (2022).

[29] S. L. Braunstein and C. M. Caves, Statistical Distance and the Geometry of Quantum States, Phys. Rev. Lett. **72**, 3439 (1994).

[30] C. W. Helstrom, Minimum mean-squared error of estimates in quantum statistics, Phys. Lett. A **25**, 101 (1967).

[31] S. L. Braunstein, C. M. Caves, and G. J. Milburn, Generalized uncertainty relations: Theory, examples, and Lorentz invariance, Ann. Phys. (NY) **247**, 135 (1996).

[32] S. Pang and T. A. Brun, Quantum metrology for a general hamiltonian parameter, Phys. Rev. A **90**, 022117 (2014).

[33] A. De Pasquale, D. Rossini, P. Facchi, and V. Giovannetti, Quantum parameter estimation affected by unitary disturbance, Phys. Rev. A **88**, 052117 (2013).

[34] D. Jaksch and P. Zoller, Creation of effective magnetic fields in optical lattices: The Hofstadter butterfly for cold neutral atoms, New J. Phys. **5**, 56 (2003).

[35] H. Miyake, G. A. Siviloglou, C. J. Kennedy, W. C. Burton, and W. Ketterle, Realizing the Harper Hamiltonian with Laser-Assisted Tunneling in Optical Lattices, Phys. Rev. Lett. **111**, 185302 (2013).

[36] N. Poli, F. Y. Wang, M. G. Tarallo, A. Alberti, M. Prevedelli, and G. M. Tino, Precision Measurement of Gravity with Cold Atoms in an Optical Lattice and Comparison with a Classical Gravimeter, Phys. Rev. Lett. **106**, 038501 (2011).

[37] T. Loftus, C. A. Regal, C. Ticknor, J. L. Bohn, and D. S. Jin, Resonant Control of Elastic Collisions in an Optically Trapped Fermi Gas of Atoms, Phys. Rev. Lett. **88**, 173201 (2002).

[38] M. Theis, G. Thalhammer, K. Winkler, M. Hellwig, G. Ruff, R. Grimm, and J. H. Denschlag, Tuning the Scattering Length with an Optically Induced Feshbach Resonance, Phys. Rev. Lett. **93**, 123001 (2004).

[39] C. Weiss and Y. Castin, Creation and Detection of a Mesoscopic Gas in a Nonlocal Quantum Superposition, Phys. Rev. Lett. **102**, 010403 (2009).

[40] T. Fogarty, A. Kiely, S. Campbell, and T. Busch, Effect of interparticle interaction in a free-oscillation atomic interferometer, Phys. Rev. A **87**, 043630 (2013).

[41] A. A. Bychek, D. N. Maksimov, and A. R. Kolovsky, NOON state of Bose atoms in the double-well potential via an excited-state quantum phase transition, Phys. Rev. A **97**, 063624 (2018).

[42] P. Naldesi, P. D. Drummond, V. Dunjko, A. Minguzzi, and M. Olshanii, Massive particle interferometry with lattice solitons: Robustness against ionization, arXiv:2201.10479.

[43] D. S. Grün, K. Wittmann W., L. H. Ymai, J. Links, and A. Foerster, Protocol designs for noon states, Commun. Phys. **5**, 1 (2022).

[44] H. M. Wiseman and G. J. Milburn, *Quantum Measurement and Control* (Cambridge University Press, Cambridge, 2009).

[45] A. Hentschel and B. C. Sanders, Efficient Algorithm for Optimizing Adaptive Quantum Metrology Processes, Phys. Rev. Lett. **107**, 233601 (2011).

[46] R. Demkowicz-Dobrzański, J. Czajkowski, and P. Sekatski, Adaptive Quantum Metrology under General Markovian Noise, Phys. Rev. X **7**, 041009 (2017).

[47] L. Pezzè and A. Smerzi, Quantum Phase Estimation Algorithm with Gaussian Spin States, PRX Quantum **2**, 040301 (2021).

[48] M. Aidelsburger, M. Atala, M. Lohse, J. T. Barreiro, B. Paredes, and I. Bloch, Realization of the Hofstadter Hamiltonian with Ultracold Atoms in Optical Lattices, Phys. Rev. Lett. **111**, 185301 (2013).

[49] A. Eckardt and E. Anisimovas, High-frequency approximation for periodically driven quantum systems from a Floquet-space perspective, New J. Phys. **17**, 093039 (2015).

[50] M. Bukov, L. D'Alessio, and A. Polkovnikov, Universal high-frequency behavior of periodically driven systems: From dynamical stabilization to Floquet engineering, Adv. Phys. **64**, 139 (2015).

[51] S. Pang and A. N. Jordan, Optimal adaptive control for quantum metrology with time-dependent Hamiltonians, Nat. Commun. **8**, 14695 (2017).

[52] A. J. Hayes, S. Dooley, W. J. Munro, K. Nemoto, and J. Dunningham, Making the most of time in quantum metrology: Concurrent state preparation and sensing, Quantum Sci. Technol. **3**, 035007 (2018).

[53] K. Gietka, L. Ruks, and T. Busch, Understanding and improving critical metrology. Quenching superradiant light-matter systems beyond the critical point, Quantum **6**, 700 (2022).

[54] N. Goldman and J. Dalibard, Periodically Driven Quantum Systems: Effective Hamiltonians and Engineered Gauge Fields, Phys. Rev. X **4**, 031027 (2014).

[55] N. Goldman, J. Dalibard, M. Aidelsburger, and N. R. Cooper, Periodically driven quantum matter: The case of resonant modulations, Phys. Rev. A **91**, 033632 (2015).

[56] C. Vitelli, N. Spagnolo, F. Sciarrino, and F. De Martini, Amplification of polarization NOON states, J. Opt. Soc. Am. B **26**, 892 (2009).

[57] T. Wasak, A. Smerzi, L. Pezzé, and J. Chwedeńczuk, Optimal measurements in phase estimation: Simple examples, Quantum Inf. Process. **15**, 2231 (2016).

[58] A. Eckardt, C. Weiss, and M. Holthaus, Superfluid-Insulator Transition in a Periodically Driven Optical Lattice, Phys. Rev. Lett. **95**, 260404 (2005).

[59] S. Krämer, D. Plankensteiner, L. Ostermann, and H. Ritsch, Quantumoptics.jl: A Julia framework for simulating open quantum systems, Comput. Phys. Commun. **227**, 109 (2018).

[60] T. Bilitewski and N. R. Cooper, Scattering theory for Floquet-Bloch states, Phys. Rev. A **91**, 033601 (2015).